Inorganic Chemistry

Article

pubs.acs.org/IC

Tetra-2,3-pyrazinoporphyrazines with Externally Appended Pyridine Rings. 15. Effects of the Pyridyl Substituents and Fused Exocyclic Rings on the UV−Visible Spectroscopic Properties of Mg(II)−Porphyrazines: A Combined Experimental and DFT/TDDFT Study

Maria Pia Donzello,*[,†] Giorgia De Mori,[†] Elisa Viola,[†] Claudio Ercolani,[†] Giampaolo Ricciardi,[‡] and Angela Rosa*[,‡]

[†]Dipartimento di Chimica, Università di Roma Sapienza, Piazzale A. Moro 5, I-00185 Roma, Italy

[‡]Dipartimento di Scienze, Università della Basilicata, Viale dell'Ateneo Lucano 10, I-85100 Potenza, Italy

Supporting Information

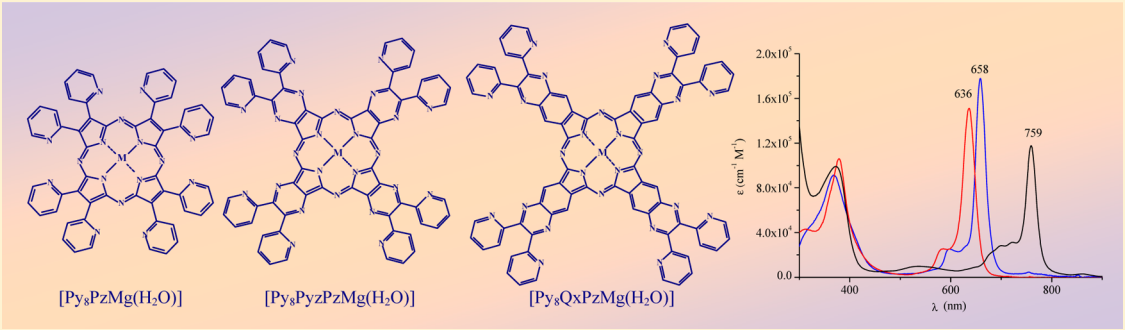

ABSTRACT: Two new Mg^{II} porphyrazine macrocycles, the octakis(2-pyridyl)porphyrazinato-magnesium(II), [$Py_8PzMg(H_2O)$], and the tetrakis-[6,7-di(2-pyridyl)quinoxalino]porphyrazinato-magnesium(II), [$Py_8QxPzMg(H_2O)$], were prepared by Mg-template macrocyclization processes, and their general physicochemical properties were examined. The previously reported porphyrazine analog, the tetrakis-2,3-[5,6-di(2-pyridyl)-pyrazino]porphyrazinato-magnesium(II), [$Py_8PyzPzMg(H_2O)$], has been also considered in the present work. The UV−visible solution spectra in nonaqueous solvents of this triad of externally octapyridinated Mg^{II} complexes exhibit the usual profile observed for phthalocyanine and porphyrazine macrocycles, with intense absorptions in the Soret (300−450 nm) and Q band (600−800 nm) regions. It is observed that the Q band maximum sensibly shifts toward the red with peak values at 635 → 658 → 759 nm along the series [$Py_8PzMg(H_2O)$], [$Py_8PyzPzMg(H_2O)$], and [$Py_8QxPzMg(H_2O)$], as the extension of the macrocycle π-system increases. TDDFT calculations of the electronic absorption spectra were performed for the related water-free model compounds [Py_8PzMg], [$Py_8PyzPzMg$], and [$Py_8QxPzMg$] to provide an interpretation of the UV−visible spectral changes occurring upon introduction of the pyrazine and quinoxaline rings at the periphery of the Pz macrocycle. To discriminate the electronic effects of the fused exocyclic rings from those of the appended 2-pyridyl rings, the UV−visible spectra of [PzMg] and [PyzPzMg] were also theoretically investigated. The theoretical results prove to agree very well with the experimental data, providing an accurate description of the UV−visible spectra. The observed spectral changes are interpreted on the basis of the electronic structure changes occurring along the series.

INTRODUCTION

Previous studies established that the series of pyrazinoporphyrazine macrocycles [$Py_8PyzPzM$] (PyzPz = tetrakis-2,3-[5,6-di(2-pyridyl)-pyrazino]porphyrazinato dianion; M = $2H^I$ or bivalent metal ion), characterized by the presence of peripheral dipyridinopyrazine fragments (Figure 1B), behave as highly electron-deficient macrocycles.[1] Exocyclic tetrametalation with formation of the pentanuclear species [$(M'Cl_2)_4Py_8PyzPzM$] (M′ = Pd^{II}, Pt^{II})[1b−e] and quaternization processes, performed with CH_3I, at the external pyridine N atoms, leading to the octacations [$(2\text{-Mepy})_8PyzPzM]^{8+}$ (neutralized by I^- ions),[1b−d,2] were observed to further increment the electron deficiency of the macrocycle. Furthermore, stepwise one-electron reductions of these systems, found to be remarkably easier than those of their parent phthalocyanine analogs, were often observed to occur as nicely reversible processes as a result of excess of negative charge redistribution capability and consequent stabilization of the reduced species formed.

Several members of the above series of mono- or pentanuclear and octationic macrocycles, mainly carrying centrally Mg^{II}, Zn^{II}, or Pd^{II}, proved to be excellent photosensitizers for the generation of singlet oxygen, $^1O_2$, the cytotoxic agent active in the anticancer curative modality

Received: April 14, 2014
Published: July 24, 2014

   dx.doi.org/10.1021/ic500880m | *Inorg. Chem.* 2014, 53, 8009−8019

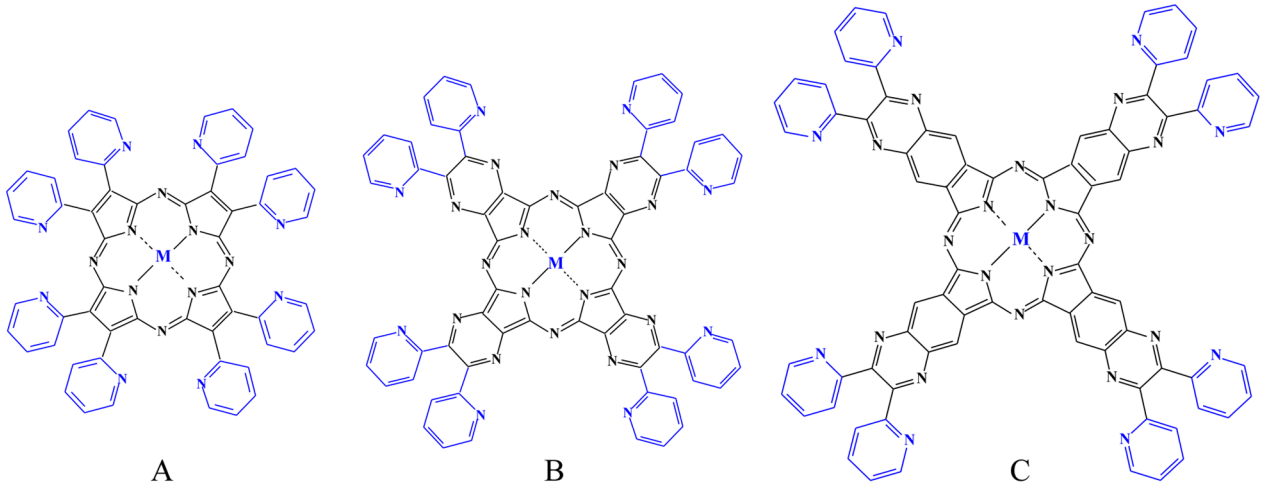

Figure 1. Schematic representation of [Py_8PzM] (A), [$Py_8PyzPzM$] (B), and [Py_8QxPzM] (C).

known as photodynamic therapy (PDT).[1c−e,3] Besides, detailed studies on the octacation [(2-Mepy)$_8$PyzPzZn]$^{8+}$ and the binuclear Zn^{II}/Pt^{II} hexacation [($PtCl_2$)(2-Mepy)$_6$$Py_2$PyzPzZn]$^{6+}$, bearing peripherally one $PtCl_2$ unit, allowed definition in the water medium, although in the presence of partial persistent aggregation, of different forms of interaction of the monomeric species with the 21-mer telomeric G-quadruplex structure (G4)[4] and with a double strand model of B-DNA,[5] making them appear promising for a more complex anticancer efficacy. Noteworthy, the Zn^{II}/Pt^{II} hexacation presents externally a cisplatin-like coordination site, $N_{2(pyr)}PtCl_2$, this reinforcing for the binuclear species multimodal anticancer potentialities.

In light of the above-mentioned studies on the pyrazinoporphyrazine complexes [$Py_8PyzPzM$], it was believed of interest to investigate the electronic effects associated with the change of the size of the π-system of the macrocycle. To this end, the synthesis of two novel series of metallomacrocycles, with formula [Py_8PzM] (Figure 1A) and [Py_8QxPzM] (Figure 1C), characterized by a different extension of the macrocycle π-system, was performed. The porphyrazine [Py_8PzM] series can be considered as derived from the pyrazinoporphyrazine analogs [$Py_8PyzPzM$] by removing the pyrazine rings. The Py_8Pz macrocycle, which bears the 2-pyridyl substituents directly attached at the β positions of the pyrrole rings, is characterized by a reduced π-system compared to that of the macrocycle Py_8PyzPz. The second type of metallomacrocycles [Py_8QxPzM] can be considered as derived from [$Py_8PyzPzM$] by interposition of a benzene ring between the pyrrole and the pyrazine rings, thus generating a more expanded π-system than in the parent species. Several analogs of the quinoxalinoporphyrazine compounds [Py_8QxPzM] carrying different external substituents were previously reported.[6]

The present contribution reports the synthesis, physicochemical properties, and solution UV−visible spectral behavior of the new macrocycles carrying centrally Mg^{II} as a Mg(H_2O) unit. To rationalize the UV−visible spectral changes observed along the [$Py_8PzMg(H_2O)$], [$Py_8PyzPzMg(H_2O)$], and [$Py_8QxPzMg(H_2O)$] triad, density functional theory (DFT) and time-dependent DFT (TDDFT) calculations of the ground and excited states of the water-free model complexes of the triad were performed. To disentangle the electronic effects of the fused exocyclic rings from those of the appended 2-pyridyl rings, the ground and excited states of the peripherally unsubstituted [PzMg] and [PyzPzMg] complexes were also investigated.

EXPERIMENTAL SECTION

Solvents and reagents were used as purchased unless otherwise specified. Pyridine was dried by refluxing over CaO. Dimethyl sulfoxide (DMSO, RPE C. Erba) was freshly distilled over CaH_2. Methanol was dried over sodium and freshly distilled before use. 2-Pyridylacetonitrile (99%) and bisublimed iodine were commercial products from Aldrich and were used without further purification. The 6,7-dicyano-2,3-di(2-pyridyl)-1,4-quinoxaline, [$(CN)_2Py_2Qx$], was prepared from 4,5-diaminophthalodinitrile and 2,2′dipyridyl as previously reported.[7] The 2,3-dicyano-pyrazine was prepared as reported in the literature.[8]

Synthesis of 1,2-Dicyano-1,2-di(2-pyridyl)-ethylene, [$(CN)_2Py_2Et$]. This compound was prepared following the previously reported procedure,[9] modified as follows: 2-Pyridylacetonitrile (3.3 mL, 0.030 mmol) and bisublimed iodine (7.5 g, 0.029 mol) were added under N_2 to a solution of methanol (10 mL) and anhydrous ether (10 mL), and the mixture was kept at room temperature for 1 h. After addition of a solution of CH_3ONa obtained by dissolving, with stirring, metallic sodium (1.4 g) in 14 mL of methanol (preliminarly distilled over Na), the resulting mixture was kept overnight in the refrigerator. After filtration, the separated brown crystalline solid was washed with cool methanol and brought to constant weight under vacuum (10^{-2} mmHg; 1.59 g, yield 45%). Calcd for [$(CN)_2Py_2Et$], $C_{14}H_8N_4$: C, 72.4; H, 3.47; N, 24.12. Found: C, 71.93; H, 3.45; N, 23.89%. UV−vis (λ, nm (logε)): CH_3OH, 212 (4.17), 222(sh) (4.10), 322 (4.22); CH_3CN, 212 (4.16), 224(sh) (4.07), 323 (4.21). IR (KBr, cm^{-1}): 2216 (w-m, ν_{CN}), 1579 (s), 1467 (s), 1438 (s), 1302 (w), 1294 (w), 1226 (w-m), 1160 (w), 1103 (m), 1055 (m), 1026 (vw), 995 (s), 974 (w), 893 (vw), 850 (vw), 781 (vvs), 737 (vs), 652 (vw), 619 (s), 580 (w), 489 (s), 470 (vs), 397 (m-s), 377 (vw), 272 (m). ^{1}H NMR (DMSO-d_6, 273 K): δ/ppm = 8.823 (ddd, J = 4.8, 1.7, 1.0 Hz, 1 H), 7.672 (ddd, J = 4.8, 7.8, 1.0 Hz, 1 H), 8.124 (ddd, J = 7.8, 7.8, 1.7 Hz, 1 H), 8.045 (ddd, J = 7.8, 1.0 Hz, 1 H). ^{13}C NMR (DMSO-d_6, 273 K): δ/ppm = 150.5 (1 H), 127.1 (1 H), 138.8 (1 H), 125.1 (1 H).

Synthesis of [$Py_8PzMg(H_2O)$]·4H_2O. A suspension of metallic magnesium (120 mg, 4.94 mmol) in propyl alcohol (15 mL), with few crystals of iodine added, was heated to reflux under stirring for 16 h. After addition of [$(CN)_2Py_2Et$] (300 mg, 1.29 mmol), the suspension was again heated to reflux for 8 h. After cooling, the solvent was left to evaporate in air, the solid residue was suspended in CH_3COOH (10%, 5 mL), and the mixture was kept under stirring for 1 h. The solid was then separated by centrifugation, washed repeatedly with water until neutrality, and brought to constant weight under vacuum. The solid was purified by column chromatography using alumina (Acros, activated, neutral, 50−200 μm) as the solid phase and a solution of

dx.doi.org/10.1021/ic500880m | Inorg. Chem. 2014, 53, 8009−8019

20% CH_3OH in $CHCl_3$ as eluant for the first column, followed by the use of a gradient from 5% to 30% of CH_3OH in $CHCl_3$ for the second column. Column chromatography was repeated using as the solid phase activated basic alumina (Merck, 70−230 mesh). The bluish Mg^{II} complex was brought to constant weight under vacuum (10^{-2} mmHg; 50 mg, yield 15%). Calcd for $[Py_8PzMg(H_2O)]\cdot 4H_2O$, $C_{56}H_{42}MgN_{16}O_5$: C, 64.47; H, 4.06; N, 21.48. Found: C, 64.54; H, 4.22; N, 20.88%. IR (KBr, cm^{-1}): 3450 (broad), 1718 (vw), 1629 (w), 1585 (s), 1508 (w), 1463 (m), 1423 (w), 1286 (vw), 1238 (w), 1149 (m), 1095 (w), 1049 (vw), 1006 (m-s), 983 (m), 881 (w), 835 (w), 786 (m), 742 (s), 665 (vw), 607 (w), 526 (vw), 497 (vw), 403 (w). ^1H NMR (DMF-d_7, 273 K): δ/ppm = 8.766 (ddd, J = 4.7, 1.8, 0.9 Hz, 1 H), 7.564 (ddd, J = 4.7, 7.6, 0.9 Hz, 1 H), 8.201 (ddd, J = 7.6, 7.6, 1.8 Hz, 1 H), 8.998 (ddd, J = 7.6, 0.9, 0.9 Hz, 1 H). ^{13}C NMR (DMF-d_7, 273 K): δ/ppm = 149.4 (1 H), 122.7 (1 H), 135.7 (1 H), 129.0 (1 H).

Synthesis of $[Py_8QxPzMg(H_2O)]\cdot 4H_2O$. Magnesium (90.4 mg, 3.72 mmol), propyl alcohol (15 mL), and a few crystals of iodine were introduced in a small flask (25 mL), and the mixture was heated to reflux under stirring for 16 h. After addition of the precursor $[(CN)_2Py_2Qx]$ (310 mg, 0.927 mmol), the mixture was heated to reflux again for 8 h. It was then brought to room temperature and poured into a vessel, and the solvent was left to evaporate completely. To the solid residue was added CH_3COOH (10%, 5 mL), and the mixture was kept under stirring for 1 h. After centrifugation, the solid residue was washed repeatedly with water, THF, and acetone and brought to constant weight under vacuum (10^{-2} mmHg; 264.2 mg, yield 81%). Calcd for $[Py_8QxPzMg(H_2O)]\cdot 4H_2O$, $C_{80}H_{50}MgN_{24}O_5$: C, 66.19; H, 3.47; N, 23.15. Found: C, 66.59; H, 3.59; N, 21.83%. IR (KBr, cm^{-1}): 3440 (broad), 1772 (vw), 1726 (vw), 1585 (s), 1566 (s), 1473 (m-s), 1383 (w), 1346 (vs), 1280 (vvw), 1248 (vw), 1145 (w), 1103 (vs), 1034 (s), 999 (m), 983 (vw), 893 (w), 875 (w-m), 839 (vvw), 821 (w), 791 (m), 746 (s), 708 (m-s), 596 (m), 548 (w), 501 (vw), 426 (vw), 403(w), 279 (vw).

Synthesis of Tetrakis-[2,3-pyrazino]porphyrazinato-magnesium(II), $[PyzPzMg(H_2O)]\cdot 3H_2O$. Magnesium (124.1 mg, 5.105 mmol), propyl alcohol (15 mL), and a few crystals of iodine were introduced in a small flask (25 mL), and the mixture was heated to reflux under stirring for 14 h. After addition of the precursor, 2,3-dicyano-pyrazine (168.5 mg, 1.295 mmol), the mixture was heated to reflux again for 8 h. It was then brought to room temperature and poured into a vessel, and the solvent was left to evaporate completely. To the solid residue was added CH_3COOH (25%, 3 mL), and the mixture was kept under stirring for 30 min. After centrifugation, the solid residue was washed repeatedly with water until neutrality and then with acetone and brought to constant weight under vacuum (10^{-2} mmHg; 193.6 mg, yield 97%). Calcd for $[PyzPzMg(H_2O)]\cdot 3H_2O$, $C_{24}H_{16}MgN_{16}O_4$: C, 46.74; H, 2.61; N, 36.33. Found: C, 47.30; H, 2.86; N, 35.13%.

NMR Measurements. NMR spectral data were obtained by dissolving the samples in 700 μL of DMF-d_7 (99.5%, CIL) or DMSO-d_6 (99.9%, Aldrich) at 27 °C. ^1H and ^{13}C experiments were performed on a Bruker AVANCE AQS 600 spectrometer operating at the proton frequency of 600.13 MHz and equipped with a Bruker multinuclear, z gradient probehead. ^1H and ^{13}C assignments were obtained by means of HSQC experiments carried out using 1024 data points in the f2 dimension and 512 data points in the f1 dimension, a recycle delay of 1 s, and a coupling constant of 150 Hz. ^1H and ^{13}C chemical shifts are reported in ppm and are referred to the residual signals (^1H = 8.03 ppm and ^{13}C = 162.5 ppm in the case of DMF-d_7 and ^1H = 2.50 ppm and ^{13}C = 39.5 ppm in the case of DMSO-d_6).

Quantum Chemical Calculations. DFT and TDDFT calculations were performed with the Amsterdam Density Functional (ADF) program package, release 2013,[10] employing the all-electron TZP basis set, which is an uncontracted triple-ζ STO basis set with one 3d polarization function for C and N, one 2p for H, and one 3p and one 3d for Mg. To preserve the high symmetry of the investigated systems (*vide infra*) and hence to reduce the computational effort, the experimentally detected axial water ligand was not considered in the calculations on $[Py_8PzMg]$, $[Py_8PyzPzMg]$, and $[Py_8QxPzMg]$. This choice is justified by previous calculations on $[TTDPzMg(H_2O)]$ (TTDPz = tetrakis(thiadiazole)porphyrazinato dianion)[11] showing that the axially ligated water molecule is hardly retained in the presence of coordinating solvents and, even though retained, has little impact, if any, on the electronic structure and the UV−visible spectral behavior of the complex. The ground state molecular structures of [PzMg] and [PyzPzMg] and of the water-free octapyridyl model complexes, $[Py_8PzMg]$, $[Py_8PyzPzMg]$, and $[Py_8QxPzMg]$, were optimized in the gas-phase using the BP86[12] exchange-correlation functional. For the octapyridyl substituted complexes D_{2d} and D_4 symmetry structures, both characterized by a ud (u = up; d = down) orientation of the N atoms of the vicinal pyridine rings (the pyridine substituents residing on the same pyrazine subunit), were theoretically explored. They were found to be nearly degenerate with the D_4 symmetry structure being slightly more stable (~1.0 kcal/mol) than the D_{2d} structure only in the case of $[Py_8PzMg]$. Therefore, we restrict the ground and excited state theoretical studies to the D_4 conformers. The D_4 symmetry conformers show the same ud-ud-ud-ud orientation of the pyridine N atoms as found in the X-ray structure of the Co^{II} complex $[Py_8PyzPzCo(DMSO)_2]$.[13] Structures with uu or dd orientation of the vicinal pyridine N atoms were not considered on the basis of our previous theoretical studies on similar complexes showing that this type of orientation of the pyridines residing on the same pyrazine ring is energetically unfavorable.[1b] Unconstrained geometry optimization of [PzMg] and [PyzPzMg] converged to D_{4h} structures, as expected. All optimized structures were verified to be true minima by frequency calculations. Vertical absorption energies and oscillator strengths of the lowest dipole allowed singlet E and A_2 excited states were computed at TDDFT level using the hybrid B3LYP[14] functional. This functional was shown to provide a reliable and accurate description of the UV−visible spectra of pyridyl substituted pyrazinoporphyrazine complexes.[3,5] Solvent (DMF) effects on the ground state electronic structure and on the excited states were modeled through a dielectric continuum model, which was chosen to be the COSMO model.[15] The calculated excitation energies contain, apart from the altered "solvated" orbitals (slow term), also the contributions from the "fast" solvent response term.[16]

Other Physical Measurements. IR spectra of the solid materials as KBr pellets were recorded in the range of 4000−250 cm^{-1} on a Varian 660-IR FT-IR spectrometer. UV−visible solution spectra were recorded with a Varian Cary 5E spectrometer by using 1 cm quartz cuvettes. Elemental analyses for C, H, and N were provided by the "Servizio di Microanalisi" at the Dipartimento di Chimica, Università (Roma) on an EA 1110 CHNS-O instrument.

RESULTS AND DISCUSSION

The Mg^{II} Complexes $[Py_8PzMg(H_2O)]$ and $[Py_8QxPzMg(H_2O)]$. *Synthesis and Characterization.* As reported in the Experimental Section, the Mg^{II} complexes $[Py_8PzMg(H_2O)]$ and $[Py_8QxPzMg(H_2O)]$ are obtained by the template cyclotetramerization of the respective precursors, $[(CN)_2Py_2Et]$ and $[(CN)_2Py_2Qx]$, in refluxing propyl alcohol in the presence of Mg^{II}-propylate. The two complexes are normally formed as hydrated species. The presence of clathrated water molecules is a common feature for porphyrazine macrocycles carrying externally annulated heterocyclic rings, as has been already repeatedly pointed out.[1] The amount of chlatrated water, which can vary significantly for different prepared batches, can be easily removed by mild heating (ca. 100 °C) under vacuum, a behavior valid also for the present Mg^{II} compounds. After the loss of water, thermogravimetric analysis shows that both Mg^{II} macrocycles are stable in an inert atmosphere at temperatures up to ca. 300 °C. Exposure of the heated samples to air leads to a rehydration of the material. Due to the modest role played by the clathrated water molecules as to the general aspects of the investigated physicochemical properties, they will be hereafter neglected in the given formulas.

dx.doi.org/10.1021/ic500880m | Inorg. Chem. 2014, 53, 8009−8019

Table 1. UV−Visible Spectral Data of the Mg(II) Porphyrazines

		λ, nm (log ε)						
compound	solvent	Soret region		Q band region				ref[a]
$[Py_8PzMg(H_2O)]$	Py	381 (4.80)	583 (4.18)	638 (4.89)				tw
	DMSO	378 (4.52)	583 (3.95)	636 (4.63)				tw
	DMF	378 (5.05)	583 (4.46)	636 (5.18)				tw
	$CHCl_3$	378 (4.74)	583 (4.10)	637 (4.80)				tw
$[Py_8PyzPzMg(H_2O)]$	Py	375 (5.23)		596 (4.65)	631sh (4.64)	658 (5.54)		3
	DMSO	374 (5.08)	566sh (3.96)	594 (4.36)	629sh (4.55)	653 (5.34)		3
	DMF	370 (4.94)		597 (4.39)	628sh (4.43)	658 (5.20)		1e
$[Py_8QxPzMg(H_2O)]$	Py	378 (5.09)	534 (4.10)	684 (4.47)	702 (4.56)	726 (4.63)	765 (5.21)	tw
	DMSO	371 (5.03)	533 (4.05)	676sh (4.40)		707sh (4.61)	756 (4.96)	tw
	DMF	373 (4.99)	535 (3.99)	677sh (4.32)	698 (4.45)	721 (4.49)	759 (5.07)	tw
	$CHCl_3$	374 (5.00)	535 (3.94)	684 (4.22)	701 (4.21)	727 (4.33)	766 (5.11)	tw
$[PyzPzMg(H_2O)]$	DMSO	331 (4.57) 365 (4.52)	576 (4.18)			633 (5.05)		tw
	DMF[b]	327 (4.59) 370 (4.61)	578 (4.19)			637 (5.10)		

[a]tw = this work. [b]Solution in DMF containing 5% DMSO.

Both the $[Py_8PzMg(H_2O)]$ and $[Py_8QxPzMg(H_2O)]$ macrocycles are formulated with one water molecule axially ligated to Mg^{II}, in line with a similar formulation for the "pyrazinoporphyrazine" complex $[Py_8PyzPzMg(H_2O)]$.[1a] The presence of such a water molecule is difficult to be proved directly, but its presence is encouraged by the fact that the $Mg(H_2O)$ moiety is commonly observed in porphyrazine and phthalocyanine macrocycles carrying Mg^{II} centrally. Single-crystal X-ray work has established the presence of this moiety in the complexes $[(omtp)Mg(H_2O)]$[17] (omtp = octakis(methylthio)-porphyrazinato dianion) and $[PcMg(H_2O)]\cdot 2py$[18] (Pc = phthalocyaninato dianion, $C_{32}H_{16}N_8^{2-}$). The presence of the same monoaquo moiety, $Mg(H_2O)$, was given some support in the previously reported Mg^{II} complexes of the tetrakis(thia/selenodiazole)porphyrazines.[19] Interestingly, even the complex $[PcMg(H_2O)_2]$, bearing two axially ligated water molecules has been reported,[20] and a dimerized monohydrate of a low-symmetry porphyrazine macrocycle has been structurally elucidated.[21] Finally, the presence of one water molecule coordinated to Mg^{II} has been recently established for a porphyrazine macrocycle carrying externally pyrrolyl and pyridylmethylamino groups.[22]

$[Py_8PzMg(H_2O)]$ is much more soluble than $[Py_8PyzPzMg(H_2O)]$ and $[Py_8QxPzMg(H_2O)]$ in nondonor ($CHCl_3$) and donor solvents (pyridine, DMSO, DMF). In the latter solvents, the highest solubility of $[Py_8PzMg(H_2O)]$, $[Py_8PyzPzMg(H_2O)]$ and $[Py_8QxPzMg(H_2O)]$ is $\sim 10^{-3}$, $\sim 10^{-4}$, and $\sim 10^{-5}$ M, respectively.

^1H and ^{13}C NMR spectra for the complex $[Py_8PzMg(H_2O)]$ could be obtained using a solution in DMF-d_7 close to saturation ($\sim 10^{-3}$ M), whereas a poor NMR response was obtained for the macrocycle $[Py_8QxPzMg(H_2O)]$, due to combined effects of low solubility and the presence of aggregation. The ^1H NMR spectrum of $[Py_8PzMg(H_2O)]$ shows only one set of four resonance peaks for the H atoms of the external pyridyl rings (Figure S2, Supporting Information), similarly to the findings for the precursor $[(CN)_2Py_2Et]$ (in DMSO-d_6, Figure S1, Supporting Information). In a comparison of the data for the two compounds reported in the Experimental Section, it is interesting to observe that, consequent to the formation of the macrocycle from the precursor, the π-ring current induces a low field shift of the γ and δ resonances peaks of the pyridyl rings, the magnitude of this shift depending upon the distances of the proton from the central macrocycle. The γ,γ′ protons are shifted by 0.077 ppm, while the δ,δ′ protons, being in the closest position to the central π-conjugated system, are shifted by 0.953 ppm. This clearly indicates that the deshielding effect of the macrocycle on the δ,δ′ protons overcomes the influence of the pyridine N atom on the α,α′ protons. As a consequence, an inversion of the position of α,α′ and δ,δ′ proton resonances is observed. These results partially parallel those obtained for the precursor 2,3-dicyano-5,6-di(2-pyridyl)-1,4-pyrazine, $[(CN)_2Py_2Pyz]$, and the corresponding macrocyclic free base $[Py_8PyzPzH_2]$.[23]

UV−Visible Spectra. The UV−visible spectral data for the investigated complexes, $[Py_8PzMg(H_2O)]$, $[Py_8PyzPzMg(H_2O)]$, and $[Py_8QxPzMg(H_2O)]$, are listed in Table 1. The spectra show in most cases, immediately or after a short time, the aspect typical of the monomeric species (narrow and intense Q(0,0) band), as exemplified in Figure 2 for DMF solutions.

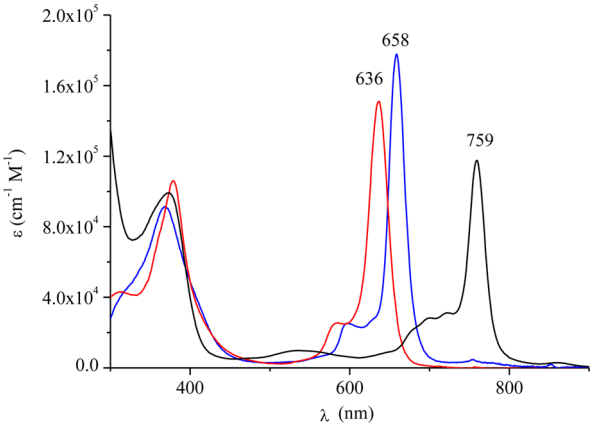

Figure 2. UV−visible spectra in DMF of $[Py_8PzMg]$ (red), $[Py_8PyzPzMg]$ (blue), and $[Py_8QxPzMg]$ (black).

The three species show in all solvents a similar spectral profile, with intense absorptions in the Soret (300−450 nm) and Q band regions (600−800 nm). These spectral features, which closely resemble those normally observed for phthalocyanine and porphyrazine macrocycles,[24] are very little sensitive to the nature of the solvent, as can be inferred from the spectral data in Table 1. It is worth noting that $[Py_8QxPzMg(H_2O)]$

dx.doi.org/10.1021/ic500880m | Inorg. Chem. 2014, 53, 8009−8019

Table 2. Selected Bond Lengths (Å) and Dihedral Angles (deg) Calculated for [PzMg] and Analogs

	[PzMg]	[Py_8PzMg]	[PyzPzMg]	[Py_8PyzPzMg]	[Py_8QxPzMg]
Mg−N_p	1.985	1.989	2.018	2.019	2.015
C−C_{py}		1.476		1.497	1.497
θ^a		54.9		55.7	53.5
φ^b	0.0	2.7	0.0	0.3	0.2
ω^c	0.0	3.8	0.0	0.5	0.2

[a]Dihedral angle between the pyridine rings and the macrocycle plane. [b]Dihedral angle between adjacent pyrrole planes (saddling). [c]Dihedral angle between opposite pyrrole planes (ruffling).

shows an *extra broad absorption* in the spectral region between the Q and B bands, regardless of the nature of the solvent. This broad absorption is similar to what has been reported previously in the spectra of alkoxy- and thioalkyl-substituted Pcs and Pzs.[25] In the case of the thioalkyl-substituted Pzs, this band has been associated with n(sulfur) → π^* transitions and n(nitrogen) → π^* transitions.[25a−d] MCD spectra indicated in this band region the presence of broad Faraday B terms.[25a] In the case of alkoxy- and thioalkyl-substituted Pcs, the broad absorption between the Q and B bands has been associated, on the basis of quantum chemical calculations, to doubly degenerate excited states dominated by transitions out of π molecular orbitals (MOs) with large amplitude on the lone pairs of the peripheral heteroatoms into the Gouterman π^* MOs.[25e,f] This assignment is supported by MCD spectra pointing to the presence of a Faraday A term in this region.[25e]

From the spectral data in Table 1 and the spectra in Figure 2, it is apparent that, while the position of the B band system changes very little, the Q bands shift to the red when moving along the triad, with the red shift being the largest for the quinoxalinoporphyrazine complex. As shown in Table 1, the average position of the Q(0,0) band in the different solvents moves to the red by 20−25 nm on going from [Py_8PzMg(H_2O)] to [Py_8PyzPzMg(H_2O)]. A much larger red shift (∼100 nm) occurs, instead, when moving from [Py_8PyzPzMg(H_2O)] to [Py_8QxPzMg(H_2O)]. Noteworthy, a practically identical bathochromic shift was observed for the couples of Zn^{II} analogs, [R_8PyzPzZn] and [R_8QxPzZn] (R = butoxycarbonyl, neopentyl, diethylamino, *tert*-butylsulfanyl, 2,6-diisopropylphenoxy).[6b]

The progressive red shift of the Q band upon increasing the extension of the macrocycle π-system shown by the investigated series of Mg^{II} complexes is reminiscent of that observed along the porphyrazine (Pz), phthalocyanine (Pc), and naphthalocyanine (Nc) series of compounds.[26,27] Sticking to the Mg^{II} derivatives, the Q(0,0) band maximum of [PzMg], [PcMg], and [NcMg] is located at 584 nm (MeOH),[28] 680 nm (ClNP),[29] and 776 nm (ClNP),[30] respectively, with a much larger global shift (192 nm) than that observed for the presently investigated series of compounds (124 nm). A more meaningful comparison between the two series of Mg^{II} complexes cannot leave apart the perturbing electronic effects of the external pyridyl rings, however. In this respect, the spectral data indicate that while for [Py_8PzMg] the Q(0,0) band is red-shifted by 51 nm with respect to [PzMg],[28] for [Py_8PyzPzMg], it is red-shifted by only 23 nm relative to the parent complex [PyzPzMg] (Q band at 635 nm in DMSO).[31] This suggests that the electronic effects of the pyridyl rings are more or less pronounced depending on the nature of the ring to which they are attached, being largest when they are appended directly to the pyrrole rings. It is worth noting that despite the red shift induced by the pyridyl substituents, the Q(0,0) band of [Py_8PyzPzMg] and [Py_8QxPzMg] experiences a 17−20 nm blue shift with respect to the corresponding Pc and Nc species, [PcMg] and [NcMg]. This observation clearly indicates that the enlargement of the π-conjugated system of the porphyrazine core is less effective when obtained by condensation of pyrazine rings or quinoxaline rings than when achieved by condensation of benzene (Pc) or naphthalene (Nc) rings.

To provide an interpretation of the spectral changes accompanying the introduction of the pyrazine or quinoxaline ring at the periphery of the Pz macrocycle, TDDFT calculations of the electronic absorption spectra in DMF solution have been performed for the water-free model compounds [Py_8PzMg], [Py_8PyzPzMg], and [Py_8QxPzMg].

Theoretical Studies. *Molecular Structure.* The relevant structural parameters computed for the water-free octapyridyl model complexes, [Py_8PzMg], [Py_8PyzPzMg], and [Py_8QxPzMg], and for the peripherally unsubstituted [PzMg] and [PyzPzMg] species are collected in Table 2. The D_4 symmetry optimized structures of the octapyridyl model complexes are displayed in Figure 3.

The calculated φ and ω values, which provide a measure of the saddling and ruffling distortion of the macrocycle, respectively, indicate that in [Py_8PzMg] the pyridyl substituents induce a small deviation from planarity of the macrocycle. This results from the necessity to relieve the repulsion between the vicinal pyridyl rings that are in this complex in closer proximity than in the other two complexes, the pyrrole C_β−C_β distance being significantly shorter than the pyrazine C2−C3 distance (1.380 vs 1.432 Å). As can be inferred from the θ values in Table 2, in all three pyridyl-substituted complexes, the pyridine rings show a pronounced tilting. Nevertheless, the conjugation between the pyridine and macrocycle π-systems is effective only in [Py_8PzMg], as indicated by the shortening of the C−C_{py} distance in this compound (Table 2).

The elongation of the Mg−N_p distance (Table 2) moving from the small ring complexes, [PzMg] and [Py_8PzMg], to the large ring complexes, [PyzPzMg], [Py_8PyzPzMg], and [Py_8QxPzMg], indicates that the fused exocyclic rings induce a sizable expansion of the porphyrazine (Pz) core.

Ground-State Electronic Structure and Optical Spectra. TDDFT calculations of the electronic absorption spectra in DMF solution were performed for [Py_8PzMg], [Py_8PyzPzMg], and [Py_8QxPzMg]. To disentangle the electronic effects of the fused exocyclic rings from those of the appended pyridyl rings, the UV−visible spectra of [PzMg] and [PyzPzMg] were also theoretically investigated in the same solvent.

Before dealing with the excited states, the ground-state electronic structure of the investigated magnesium tetrapyrroles is briefly discussed, taking [PzMg] as a reference. An energy level scheme of the highest occupied and lowest unoccupied Kohn−Sham orbitals of [PzMg] and related macrocycles is shown in Figure 4. The plots of the two occupied and two

dx.doi.org/10.1021/ic500880m | Inorg. Chem. 2014, 53, 8009−8019

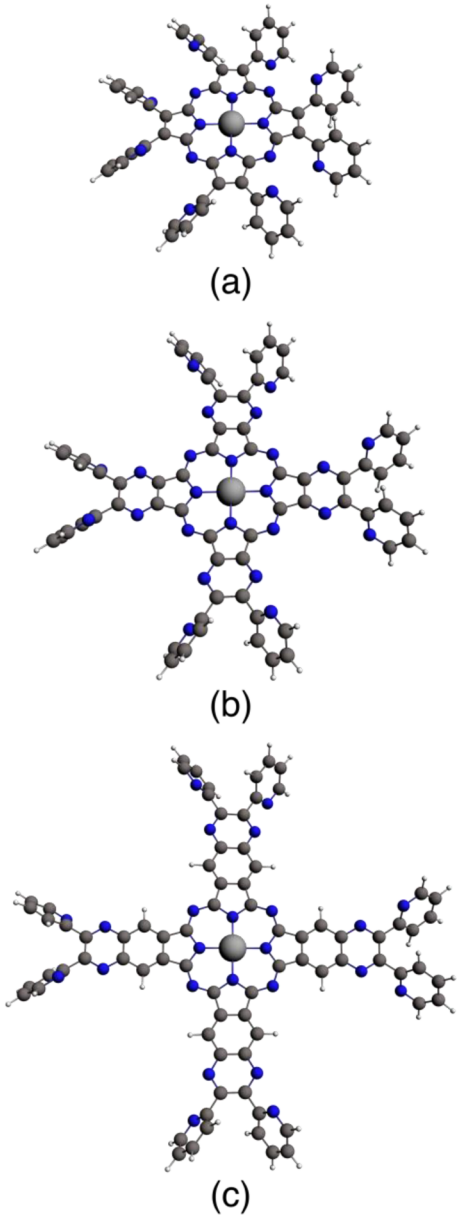

Figure 3. Top views of the D_4 symmetry optimized structures of (a) [Py_8PzMg], (b) [$Py_8PyzPzMg$], and (c) [$Py_8QxPzMg$].

unoccupied Gouterman molecular orbitals (MOs) of the investigated series of Mg^{II} tetrapyrroles are displayed in Figure 5.

The two highest occupied and the two lowest unoccupied degenerate MOs of [PzMg] are the well-known Gouterman MOs.[32] Just below the "a_{2u}-derived" $10a_2$ orbital, there is a set of four MOs, three of which, the $10b_2$, 21e, and $9a_2$, are π orbitals of the Pz macrocycle with large amplitude on the C_β atoms and the fourth, the $9b_2$, is a σ orbital of the Pz skeleton.

The level scheme of [Py_8PzMg] in Figure 4 shows that the appended pyridyl rings at the C_β positions slightly destabilize the two occupied Gouterman MOs. The unoccupied degenerate pair of Gouterman MOs stay put, instead, to the effect that the HOMO/LUMO gap is 0.12 eV smaller in [Py_8PzMg] than in the parent [PzMg]. The pyridyl substituents also introduce additional MOs between the occupied Gouterman levels. These are the $30b_2$, 60e, and $30a_2$, which are brought about by antibonding interactions between the π orbitals of the porphyrazine macrocycle having large amplitude on the C_β atoms ($10b_2$, 21e, and $9a_2$) and the pyridyl π orbitals.

More pronounced is the impact of the fused pyrazine rings on the electronic structure of [PzMg]. As apparent from the level scheme of Figure 4, the fused pyrazine rings stabilize all levels, due to the increased nuclear charge. The only exception is the $21a_1$ HOMO whose stabilization is counteracted by the destabilizing effect of the antibonding between the pyrazine and the pyrrole rings (see the plot of the $21a_1$ in Figure 5). Some antibonding between the pyrazine and the pyrrole rings is also present in the unoccupied Gouterman MOs, the 35e (see the plots of the 35:xz and 35e:yz components in Figure 5). These MOs are, however, much less destabilized than the HOMO because each component of the degenerate pair feels the antibonding effect of only two of the four fused pyrazine rings. As a result, the two unoccupied Gouterman MOs are only slightly less stabilized than the "a_{2u}-derived" $16a_2$ MO. Therefore, pyrazine annulation of the porphyrazine macrocycle reduces the HOMO/LUMO gap and increases the separation between the two occupied Gouterman MOs.

When we compare the one-electron levels of [PyzPzMg] to those of its pyridyl derivative, [$Py_8PyzPzMg$], it is apparent that the externally appended pyridyl rings have only a minor impact on the position of the Gouterman MOs. This is not surprising in view of the negligible π-conjugation between the pyridyl substituents and the pyrazine rings. Actually, the unoccupied Gouterman MOs are only slightly stabilized by the externally appended pyridyl groups, indicating, by the way, that the electron-deficient character of the pyridyl substituted pyrazinoporphyrazine complexes is only marginally imputable to the pyridyl substituents.

According to the one-electron levels of Figure 4, in [$Py_8PyzPzMg$] the external pyridyl rings introduce between the occupied Gouterman levels a set of three MOs (the $36b_2$, 74e, and $36a_2$), just as observed in [Py_8PzMg]. These MOs are brought about by antibonding interactions between the pyridine π-system and the π orbitals of the pyrazinoporphyrazine macrocycle having large amplitude on the pyrazine C2 and C3 atoms. At lower energy and immediately above the "a_{2u}-derived" $42a_2$, there is an additional set of closely spaced levels. These are σ MOs localized on the pyrazine or on the pyridine rings.

In [$Py_8QxPzMg$], the weakly electron-releasing benzo rings destabilize all levels but preferentially the highest occupied and lowest unoccupied Gouterman MOs, as can be seen in the level scheme of Figure 4. The bridging benzo rings also introduce in the virtual spectrum additional low-lying π^* levels, such as the 89e, $43a_2$, and $43b_2$. These MOs are highly delocalized, as can be inferred from the representative plots of the 89e components in Figure 6.

The preferential destabilization of the $48a_1$ HOMO and 88e LUMOs fits in with the antibonding, visible in the plots of these MOs in Figure 5, between the bridging benzo rings and both the pyrrole and pyrazine rings. The LUMOs are destabilized less than the HOMO, though. This is because each component of the 88e degenerate pair feels the antibonding effect of only two bridging benzo rings. Due to the differential destabilization of the HOMO and LUMOs, the HOMO/LUMO gap is in [$Py_8QxPzMg$] the smallest along the series of the investigated complexes. The level pattern of [$Py_8QxPzMg$] in Figure 4 shows that the "a_{2u}-derived" $41a_2$ is not much affected by the bridging benzo rings. This is not surprising as this MO is largely localized on the aza bridges and the pyrrolic nitrogens in

dx.doi.org/10.1021/ic500880m | Inorg. Chem. 2014, 53, 8009−8019

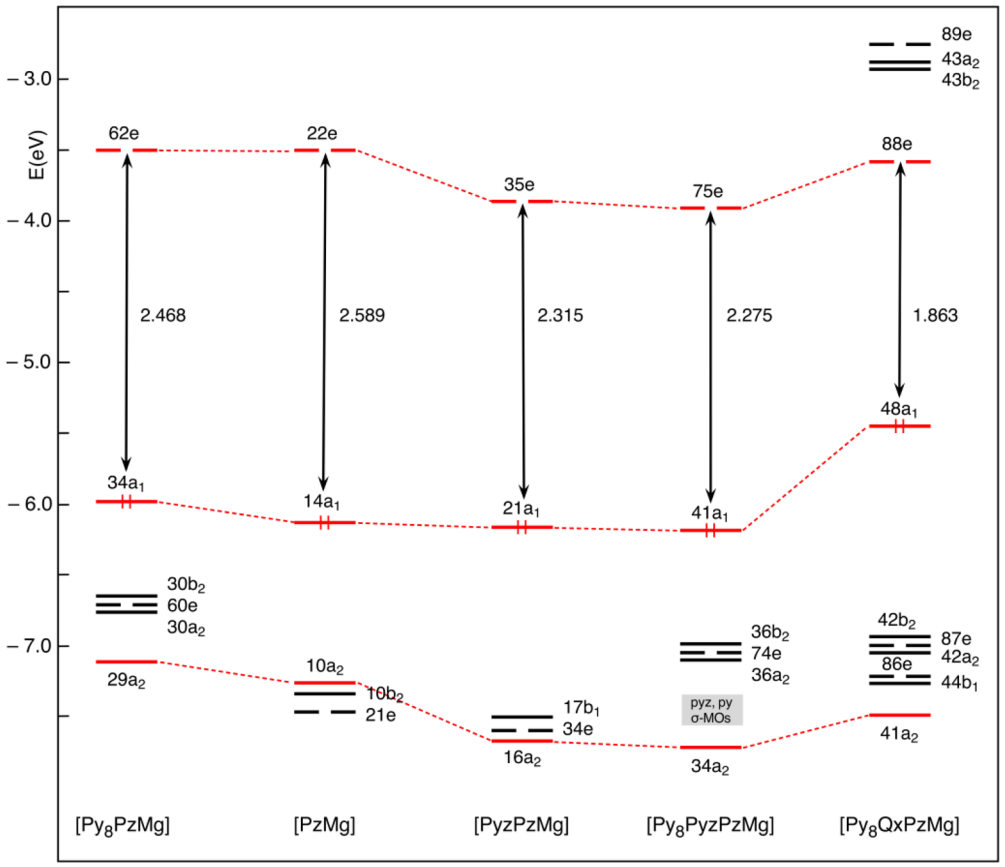

Figure 4. Energy levels of [PzMg] and derivatives computed at B3LYP/TZP level of theory in DMF solution (ε = 39.48). The Gouterman-derived MOs are indicated with red lines. For the sake of homogeneity, the MOs of [PzMg] and [PyzPzMg] are labeled according to the D_4 symmetry irreducible representations.

[Py_8QxPzMg], and in the other complexes of the series as well (see the plots of the pertinent MOs in Figure 5), and, as such, it can only feel the destabilizing effect of the weakly electron-releasing benzo rings.

It is seen now how the described electronic structure changes following the annulation of the porphyrazine macrocycle by exocyclic rings, and the introduction of peripheral pyridyl groups reflect on the UV−visible spectroscopic properties of the investigated series of complexes.

The excitation energies and oscillator strengths calculated for the lowest singlet excited states of [PzMg] and derivatives are reported in Tables 3−5, together with the major one-electron transitions contributing to the excited-state solution vectors. In Figure 7 and Figure S3 in the Supporting Information the electronic absorption spectra computed for [Py_8PzMg], [Py_8PyzPzMg], and [Py_8QxPzMg] in DMF solution are compared with the experimental ones. Only the results obtained for the E excited states are discussed in the following. The A_2 excitations have oscillator strengths smaller than 3.0×10^{-3} and are not relevant to the interpretation of the main spectral features of the investigated compounds. Considering first [PzMg] as point of reference, TDDFT calculations (Table 3) predict only one excited state in the energy regime of the Q bands. This is the intense 1^1E state, computed at 2.22 eV (559 nm), slightly to the blue of the Q(0,0) band appearing at 2.12 eV (584 nm) in the MeOH solution spectrum of [PzMg][28,31] and at 2.08 eV (594 nm) in the hexane solution spectrum of [OEPzMg] (OEPz = octaethylporphyrazine).[32] The 1^1E state is mainly (82%) described by the $14a_1 \rightarrow 22e$ HOMO → LUMO transition, the higher lying Gouterman transition, the $10a_2 \rightarrow 22e$, entering with only minor weight (10%), on account of the lifting of the (near-)degeneracy of the two highest occupied Gouterman MOs in porphyrazine complexes.[33] The intense 3^1E and 5^1E states computed at 3.34 eV (371 nm) and 3.69 eV (336 nm) nicely account for the B and N bands appearing in the spectrum of [OEPzMg] at 3.31 eV (375 nm) and 3.61 eV (343 nm).[32] These excited states have a large oscillator strength because they are dominated by one-electron transitions with large transition dipole moment. The 3^1E is dominated by the $10a_2 \rightarrow 22e$ Gouterman transition; the higher lying 5^1E state is largely described by a transition out of the $9a_2$, a low-lying π MO mainly localized on the C_β atoms, into the Gouterman 22e.

Coming to [Py_8PzMg], in the energy regime of the Q bands, TDDFT calculations predict, just as for the parent [PzMg], only one excited state, the 1^1E (Table 3). This state, which is a nearly pure (94%) HOMO → LUMO state, well accounts for the energy and intensity of the Q(0,0) band appearing at 635 nm (1.95 eV) in the UV−visible spectrum of [Py_8PzMg] in DMF solution (Figures 2 and 7). In [Py_8PzMg], the 1^1E state is computed at longer wavelength and with larger oscillator strength than in [PzMg], in very nice agreement with the experiment. The predicted and observed red shift of the Q(0,0) band upon introduction of the pyridyl substituents is in line with the diminished HOMO/LUMO gap in [Py_8PzMg]. In turn, the intensification of the Q state in the pyridyl derivative is a consequence of the less effective mixing of the contributing Gouterman transitions, that leads to a less effective cancellation of their large dipole moments.

dx.doi.org/10.1021/ic500880m | Inorg. Chem. 2014, 53, 8009−8019

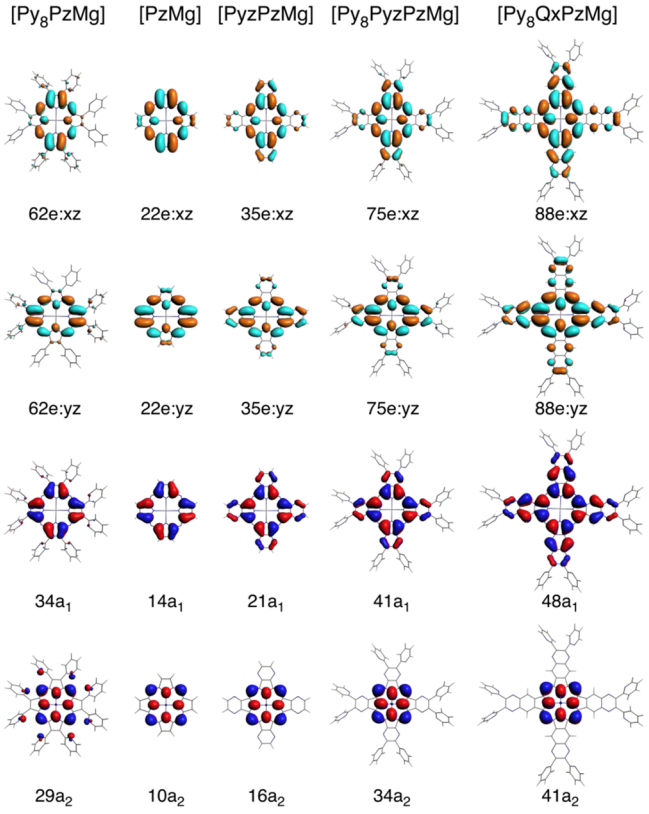

Figure 5. Plots of the Gouterman-derived MOs of [PzMg] and derivatives. For sake of homogeneity, the MOs of [PzMg] and [PyzPzMg] are labeled according to the D_4 symmetry irreducible representations.

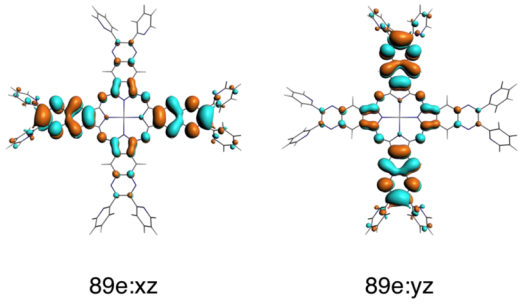

Figure 6. Plots of the two components of the 89e MO of [Py_8QxPzMg].

More relevant is the impact of the appended pyridyl rings on the B−N band system. Two intense excited states are predicted in the B−N band region of [Py_8PzMg], just as found in [PzMg] (Table 3). These are the 3^1E and 5^1E states computed at 2.74 eV (452 nm) and 3.17 eV (391 nm) and with oscillator strength of 0.7018 and 2.070, respectively. Of these, the 3^1E is an almost pure $30a_2 \rightarrow 62e$ state; the higher lying and most intense 5^1E is manly (84%) described by the $29a_2 \rightarrow 62e$ Gouterman transition. Based on their nature, and by analogy with [PzMg], the 5^1E can be identified as a B state and the 3^1E as an N state. Thus, in [Py_8PzMg], the N state is computed to the red of the B state rather than to the blue, as in the case of [PzMg]. This is not surprising because the MO from which the one-electron transition dominating the N state originates ($30a_2$) is in the pyridyl derivative destabilized by the antibonding with the appended pyridyl rings and ends up above the "a_{2u}-derived" $29a_2$ Gouterman MO. The energy and intensity of the B state, the 5^1E, very well account for the absorption maximum seen at 376 nm (3.30 eV) in the DMF solution spectrum of [Py_8PzMg]. The lower lying, less intense 3^1E excited state contributes to the red tail of the broad B band absorption.

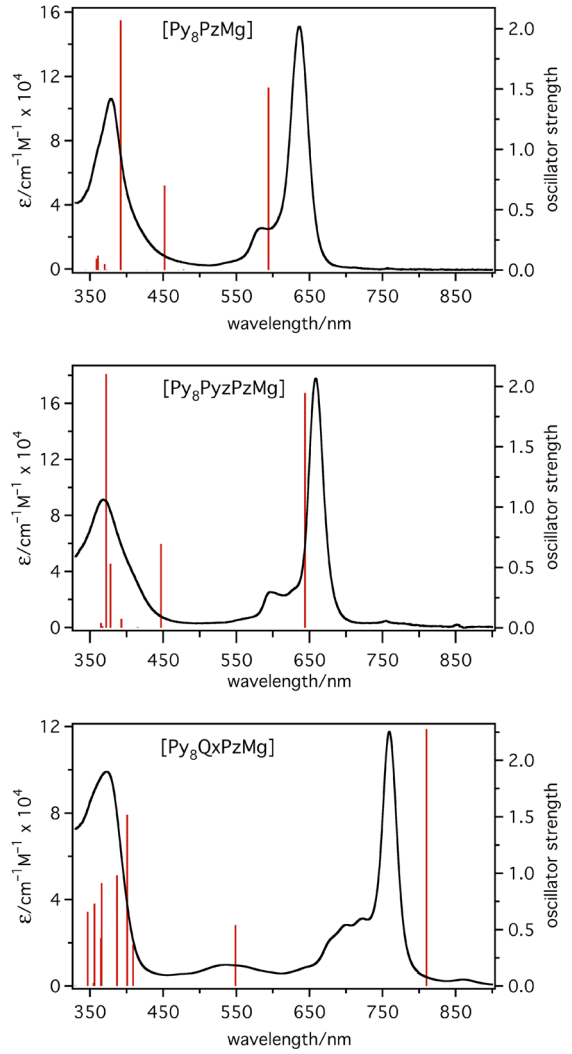

Figure 7. Comparison between computed (TDDFT/B3LYP/TZP) and experimental UV−visible absorption spectra of [Py_8PzMg], [Py_8PyzPzMg], and [Py_8QxPzMg] in DMF solution.

As for [PyzPzMg], the UV−visible spectral data in Table 1 show that Pz annulation by pyrazine rings significantly shifts the Q band to the red. In line with this observation, the excited state accounting for the Q(0,0) band, the 1^1E state, is computed in [PyzPzMg] (Table 4) 70 nm to longer wavelength than that in [PzMg], in very nice agreement with the experiment. We note, in passing, that previous TDDFT calculations on [PyzPzMg] significantly underestimated the Q band maximum.[34] However, in these calculations a pure GGA functional (PBE)[35] in conjunction with a double numeric polarization basis set[36] was used, and solvent effects were neglected.

Because the Q state in [PyzPzMg] and [PzMg] is dominated by the HOMO → LUMO Gouterman transition, the red shift of this state parallels the diminished HOMO/LUMO gap following Pz annulation.

dx.doi.org/10.1021/ic500880m | Inorg. Chem. 2014, 53, 8009−8019

Table 3. Composition, Vertical Excitation Energies [E (eV/nm)], and Oscillator Strengths (f) for the Lowest Allowed Excited States of [PzMg] and its Octapyridyl Derivative [Py_8PzMg][a]

state	composition (%)	E	f
		[PzMg][b]	
1^1E	$14a_1 \rightarrow 22e$ (82)	2.22/559 (Q)	1.110
	$10a_2 \rightarrow 22e$ (10)	*(584)*[c]; *(596)*[d]	
2^1E	$10b_2 \rightarrow 22e$ (75)	3.12/397	0.292
	$10a_2 \rightarrow 22e$ (14)		
3^1E	$10a_2 \rightarrow 22e$ (62)	3.34/371 (B)	1.094
	$10b_2 \rightarrow 22e$ (19)	*(375)*[d]	
5^1E	$9a_2 \rightarrow 22e$ (86)	3.69/336 (N)	1.373
	$10a_2 \rightarrow 22e$ (6)	*(343)*[d]	
		[Py_8PzMg]	
1^1E	$34a_1 \rightarrow 62e$ (94)	2.09/593 (Q)	1.513
2^1E	$30b_2 \rightarrow 62e$ (93)	2.59/479	0.7042×10^{-2}
3^1E	$30a_2 \rightarrow 62e$ (92)	2.74/452 (N)	0.7018
4^1E	$29b_2 \rightarrow 62e$ (92)	2.90/428	0.3144×10^{-2}
5^1E	$29a_2 \rightarrow 62e$ (84)	3.17/391 (B)	2.070
8^1E	$28a_2 \rightarrow 62e$ (34)	3.43/361	0.1206
	$29b_1 \rightarrow 62e$ (28)		
	$33a_1 \rightarrow 62e$ (22)		
9^1E	$28a_2 \rightarrow 62e$ (46)	3.45/359	0.9590×10^{-1}
	$29b_1 \rightarrow 62e$ (33)		
	$33a_1 \rightarrow 62e$ (14)		

[a]Computed at B3LYP/TZP level in DMF at the BP86/TZP gas-phase optimized geometry; only the excitations with $f > 3.0 \times 10^{-3}$ are reported. [b]For sake of homogeneity, the excited states and MOs of [PzMg] are labeled according to the D_4 symmetry irreducible representations. [c]MeOH solution spectrum of [PzMg], from ref 31. [d]Hexane solution spectrum of [OEPzMg], from ref 32.

Table 4. Composition, Vertical Excitation Energies, E (eV/nm), and Oscillator Strengths, f, for the Lowest Allowed Excited States of [PyzPzMg] and Its Octapyridyl Derivative [Py_8PyzPzMg][a]

state	composition (%)	E	f
		[PyzPzMg][b]	
1^1E	$21a_1 \rightarrow 35e$ (84)	1.97/629 (Q)	1.634
		(637)[c]	
3^1E	$16b_2 \rightarrow 35e$ (56)	3.18/390	0.276
	$16a_2 \rightarrow 35e$ (19)		
	$21a_1 \rightarrow 36e$ (17)		
5^1E	$21a_1 \rightarrow 36e$ (78)	3.29/376	0.300
	$16b_2 \rightarrow 35e$ (19)		
7^1E	$16a_2 \rightarrow 35e$ (63)	3.43/361 (B)	1.524
	$16b_2 \rightarrow 35e$ (19)	*(370)*[c]	
8^1E	$15a_2 \rightarrow 35e$ (90)	3.51/353	1.230
		(327)[c]	
		[Py_8PyzPzMg]	
1^1E	$41a_1 \rightarrow 75e$ (97)	1.92/646 (Q)	1.947
3^1E	$36a_2 \rightarrow 75e$ (90)	2.77/448	0.6964
4^1E	$37b_1 \rightarrow 75e$ (85)	2.99/415	0.4636×10^{-2}
5^1E	$41a_2 \rightarrow 76e$ (93)	3.15/393	0.7466×10^{-1}
7^1E	$33b_2 \rightarrow 75e$ (58)	3.28/378	0.5312
	$34b_2 \rightarrow 75e$ (14)		
	$34a_2 \rightarrow 75e$ (14)		
8^1E	$34a_2 \rightarrow 75e$ (61)	3.34/371 (B)	2.104
	$33b_2 \rightarrow 75e$ (22)		

[a]Computed at B3LYP/TZP level in DMF at the BP86/TZP gas-phase optimized geometry; only the excitations with $f > 3.0 \times 10^{-3}$ are reported. [b]For sake of homogeneity the excited states and MOs of [PyzPzMg] are labeled according to the D_4 symmetry irreducible representations. [c]DMF solution spectrum of [PyzPzMg], this work (see Table 1).

The energy, intensity, and composition of the 7^1E excited state (Table 4) leave no doubt on the assignment of this state to the B band maximum appearing at 370 nm in the DMF solution spectrum of the complex (see Table 1). This state is largely described by the $16a_2 \rightarrow 35e$ Gouterman transition. The lower lying and less intense 3^1E and 5^1E excited states have a $\pi \rightarrow \pi^*$ character and contribute to the red tail of the B band. The intense feature to the blue of the B band peaking at 327 nm is assigned to the intense 8^1E $\pi \rightarrow \pi^*$ state.

The excitation energies and oscillator strength computed for the excited states accounting for the Q and B bands of [Py_8PyzPzMg], the 1^1E and 8^1E, respectively, indicate that the introduction of the pyridyl groups at the periphery of [PyzPzMg] slightly shifts to longer wavelength and intensifies both the Q and B bands. The composition of the Q and B states in terms of one-electron transitions fully accounts for the red shift and intensification of these states on going from [PyzPzMg] to the pyridyl derivative. As can be inferred from the UV−visible spectra in Figure 7, there is an excellent agreement between the calculated and experimental band maxima. Additional $\pi \rightarrow \pi^*$ excited states are computed to the red of the B band maximum, with two of these, the 3^1E and 7^1E, having sizable intensity. These states well account for the considerable broadening of the red tail of the B band in this complex.

Finally, coming to [Py_8QxPzMg], the Q(0,0) band maximum appearing at 759 nm (1.63 eV) in the DMF solution spectrum of the complex (Figure 2) is satisfactorily accounted for by the intense 1^1E state that is entirely composed by the HOMO → LUMO Gouterman transition. The observed and theoretically predicted red shift of the Q band along the series [Py_8PzMg], [Py_8PyzPzMg], and [Py_8QxPzMg] reflects the progressive decrease of the HOMO/LUMO gap. In the spectral region between the Q and B bands, the calculations predict a relatively intense excited state, the 2^1E, which is dominated by a transition out of the HOMO into one of the additional low-lying π^* MOs introduced by the bridging benzo rings, the 89e (see the level diagram of Figure 4). The 2^1E state, which is computed at 549 nm and has no counterpart in the other complexes of the series, nicely accounts for most of the intensity of the *extra broad absorption* appearing at 535 nm in the DMF solution spectrum of [Py_8QxPzMg(H_2O)] (Figure 2). In the energy regime of this broad absorption, the calculations also predict a very weak ($f = 6.6 \times 10^{-5}$), z-polarized excited state, the 1^1A_2, computed at 579 nm. Similar to the 2^1E, this state is dominated by a transition out of the HOMO into one of the additional low-lying π^* MOs introduced by the bridging benzo rings, the involved MO being the $43a_2$ (see Figure 4) in this case. Thus, according to the TDDFT results, the *extra broad absorption* appearing at 535 nm in the DMF solution spectrum of [Py_8QxPzMg(H_2O)], although reminiscent of the broad absorption lying between the Q and B bands in the spectra of alkoxy- and thioalkyl-substituted Pcs and Pzs, has a different electronic origin. In the spectral region of the B band peaking at 373 nm, the calculations predict six excited states, four of which, the 4^1E, 5^1E, 6^1E, and 8^1E, account for most of the intensity of this

dx.doi.org/10.1021/ic500880m | Inorg. Chem. 2014, 53, 8009−8019

band. As can be inferred from their composition in Table 5, the most intense state, the 4^1E, is dominated by a transition out of

Table 5. Composition, Vertical Excitation Energies, *E* (eV/nm), and Oscillator Strengths, *f*, for the Lowest Allowed Excited States of [$Py_8QxPzMg$][a]

state	composition (%)	*E*	*f*
1^1E	$48a_1 \rightarrow 88e$ (99)	1.53/810 (Q)	2.277
2^1E	$48a_1 \rightarrow 89e$ (99)	2.26/549	0.5405
3^1E	$42b_2 \rightarrow 88e$ (92)	3.03/409	0.3674
4^1E	$42a_2 \rightarrow 88e$ (94)	3.09/401	1.519
5^1E	$44b_1 \rightarrow 88e$ (91)	3.20/387	0.9816
6^1E	$41a_2 \rightarrow 88e$ (37)	3.39/366 (B)	0.9139
	$48a_1 \rightarrow 90e$ (25)		
7^1E	$43b_1 \rightarrow 88e$ (21)	3.40/365	0.4259
	$47a_1 \rightarrow 88e$ (17)		
	$41a_2 \rightarrow 88e$ (14)		
	$48a_1 \rightarrow 90e$ (12)		
8^1E	$48a_1 \rightarrow 90e$ (49)	3.48/356	0.7317
	$41a_2 \rightarrow 88e$ (22)		

[a]Computed at B3LYP/TZP level in DMF at the BP86/TZP gas-phase optimized geometry; only the excitations with $f > 3.0 \times 10^{-3}$ are reported.

the highly delocalized $42a_2$ π orbital into the LUMOs. The less intense 5^1E, 6^1E, and 8^1E states arise from the mixing of the $41a_2 \rightarrow 88e$ Gouterman transition with other $\pi \rightarrow \pi^*$ transitions.

CONCLUSIONS

The studied Mg^{II} porphyrazine complexes [$Py_8PzMg(H_2O)$], [$Py_8PyzPzMg(H_2O)$], and [$Py_8QxPzMg(H_2O)$], all sharing as common structural features the presence of externally appended 2-pyridyl rings and of one water molecule axially coordinated to Mg^{II}, are characterized by a progressive enlargement of the macrocycle π-system. The explored UV−visible spectral behavior in DMF solution indicates that the Q band position for the above three species moves in the sequence 635 → 658 → 759 nm, for a total change of 124 nm. To provide an interpretation of the UV−visible spectral changes following the introduction of the pyrazine or quinoxaline ring at the periphery of the Pz macrocycle, TDDFT calculations of the electronic absorption spectra in DMF solution have been performed for the water-free model compounds [Py_8PzMg], [$Py_8PyzPzMg$], and [$Py_8QxPzMg$].

To discriminate the electronic effects of the fused exocyclic rings from those of the appended pyridine rings, the UV−visible spectra of [PzMg] and [PyzPzMg] have also been theoretically investigated in the same solvent. The theoretical results proved to agree very well with the experimental data, providing an accurate description of the UV−visible spectra. The observed spectral changes were interpreted on the basis of the electronic structure changes occurring along the series. It is found that the red shift of the Q band along the triad [Py_8PzMg], [$Py_8PyzPzMg$], and [$Py_8QxPzMg$] is related to the decrease of the HOMO/LUMO gap, which is largest in [$Py_8QxPzMg$]. The fused pyrazine rings *stabilize* the HOMO and LUMOs, but especially the latter. In contrast, the fused quinoxaline rings *destabilize* the HOMO and LUMOs, but especially the former, due to the antibonding of the bridging benzo rings with both the pyrrole and pyrazine rings. The *extra broad absorption* appearing between the Q and B bands in the spectrum of [$Py_8QxPzMg(H_2O)$] is interpreted in terms of a transition out of the HOMO into one of the additional low-lying π^* MOs introduced by the bridging benzo rings. The pyridyl substituents have a modest impact on the electronic spectra when appended to the pyrazine rings, as in [$Py_8PyzPzMg(H_2O)$] and [$Py_8QxPzMg(H_2O)$], while they induce an appreciable red shift of the Q band when attached directly to the pyrroles of the Pz ring, due to a sizable π-conjugation with the porphyrazine macrocycle.

ASSOCIATED CONTENT

Supporting Information

^{1}H NMR spectrum in DMSO-d_6 of [$(CN)_2Py_2Et$], ^{1}H NMR spectrum in DMF-d_7 of [$Py_8PzMg(H_2O)$], calculated (TDDFT/B3LYP/TZP) absorption spectra of [Py_8PzMg], [$Py_8PyzPzMg$], and [$Py_8QxPzMg$] in DMF compared with the experimental UV−visible absorption spectra measured in DMF solution, and list of the optimized coordinates and harmonic frequencies of all investigated compounds. This material is available free of charge via the Internet at http://pubs.acs.org.

AUTHOR INFORMATION

Corresponding Authors

*E-mail: mariapia.donzello@uniroma1.it.

*E-mail: angela.rosa@unibas.it.

Notes

The authors declare no competing financial interest.

ACKNOWLEDGMENTS

Financial support by the Università di Roma Sapienza and Università della Basilicata is gratefully acknowledged. The authors thank Prof. L. Mannina for useful discussions.

REFERENCES

(1) (a) Donzello, M. P.; Ou, Z.; Dini, D.; Meneghetti, M.; Ercolani, C.; Kadish, K. M. *Inorg. Chem.* **2004**, *43*, 8637. (b) Donzello, M. P.; Viola, E.; Xiaohui, C.; Mannina, L.; Rizzoli, C.; Ricciardi, G.; Ercolani, C.; Kadish, K. M.; Rosa, A. *Inorg. Chem.* **2008**, *47*, 3903. (c) Donzello, M. P.; Viola, E.; Cai, X.; Mannina, L.; Ercolani, C.; Kadish, K. M. *Inorg. Chem.* **2010**, *49*, 2447. (d) Donzello, M. P.; Viola, E.; Mannina, L.; Barteri, M.; Fu, Z.; Ercolani, C. *J. Porphyrins Phthalocyanines* **2011**, *15*, 984. (e) Donzello, M. P.; Viola, E.; Ercolani, C.; Fu, Z.; Futur, D.; Kadish, K. M. *Inorg. Chem.* **2012**, *51*, 12548.

(2) Bergami, C.; Donzello, M. P.; Monacelli, F.; Ercolani, C.; Kadish, K. M. *Inorg. Chem.* **2005**, *44*, 9862.

(3) Donzello, M. P.; Viola, E.; Bergami, C.; Dini, D.; Ercolani, C.; Giustini, M.; Kadish, K. M.; Meneghetti, M.; Monacelli, F.; Rosa, A.; Ricciardi, G. *Inorg. Chem.* **2008**, *47*, 8757.

(4) (a) Manet, I.; Manoli, F.; Donzello, M. P.; Viola, E.; Andreano, G.; Masi, A.; Cellai, L.; Monti, S. *Org. Biomol. Chem.* **2011**, *9*, 684. (b) Donzello, M. P.; Vittori, D.; Viola, E.; Manet, I.; Mannina, L.; Cellai, L.; Monti, S.; Ercolani, C. *Inorg. Chem.* **2011**, *50*, 7391. (c) Manet, I.; Manoli, F.; Donzello, M. P.; Ercolani, C.; Vittori, D.; Cellai, L.; Masi, A.; Monti, S. *Inorg. Chem.* **2011**, *50*, 7403.

(5) Manet, I.; Manoli, F.; Donzello, M. P.; Viola, E.; Masi, A.; Andreano, G.; Ricciardi, G.; Rosa, A.; Cellai, L.; Ercolani, C.; Monti, S. *Inorg. Chem.* **2013**, *52*, 321.

(6) (a) Lukyanets, E. V.; Nemikyn, V. *J. Porphyrins Phthalocyanines* **2010**, *14*, 1−40. (b) Novakova, V.; Zimcik, P.; Mietin, M.; Kopecky, K.; Musil, Z. *Eur. J. Org. Chem.* **2010**, 732. (c) Zimcik, P.; Miletin, M.; Radilova, H.; Novakova, V.; Kopecky, K.; Svec, J.; Rudolf, E. *Photochem. Photobiol.* **2010**, *86*, 168. (d) Musil, Z.; Zimcik, P.; Miletin, M.; Kopecky, K.; Lenco, J. *Eur. J. Org. Chem.* **2007**, 4535.

(7) Haas, M.; Liu, S.; Neels, A.; Decurtins, S. *Eur. J. Org. Chem.* **2006**, *24*, 5467.
(8) Popp, F. D. *J. Heterocycl. Chem.* **1974**, *11*, 79.
(9) Piechucki, C.; Michalski, J. *Bull. Acad. Polym. Sci., Ser. Sci. Chim.* **1970**, *18*, 605.
(10) (a) Amsterdam Density Functional; Scientific Computing & Modelling (SCM), Theoretical Chemistry, Vrije Universiteit: Amsterdam, The Netherlands. (URL: http://www.scm.com). (b) Baerends, E. J.; Ellis, D. E.; Ros, P. *Chem. Phys.* **1973**, *2*, 41. (c) Fonseca Guerra, C.; Snijders, J. G.; te Velde, G.; Baerends, E. J. *Theor. Chem. Acc.* **1998**, *99*, 391. (d) te Velde, G.; Bickelhaupt, F. M.; Baerends, E. J.; Fonseca Guerra, C.; van Gisbergen, S. J. A.; Snijders, J. G.; Ziegler, T. *J. Comput. Chem.* **2001**, *22*, 931.
(11) Donzello, M. P.; Ercolani, C.; Kadish, K. M.; Ricciardi, G.; Rosa, A.; Stuzhin, P. A. *Inorg. Chem.* **2007**, *46*, 4145.
(12) (a) Becke, A. D. *J. Chem. Phys.* **1988**, *88*, 1053. (b) Perdew, J. P.; Wang, Y. *Phys. Rev. B* **1986**, *33*, 8800.
(13) Viola, E.; Donzello, M. P.; Ciattini, S.; Portalone, G.; Ercolani, C. *Eur. J. Inorg. Chem.* **2009**, 1600.
(14) (a) Becke, A. D. *J. Chem. Phys.* **1993**, *98*, 5648. (b) Lee, C.; Yang, W.; Parr, R. G. *Phys. Rev. B* **1988**, *37*, 785.
(15) (a) Klamt, A.; Schürmann, G. *J. Chem. Soc., Perkin Trans.* **1993**, *2*, 799. (b) Klamt, A. *J. Phys. Chem.* **1995**, *99*, 2224. (c) Klamt, A.; Jonas, V. *J. Chem. Phys.* **1996**, *105*, 9972. (d) Pye, C. C.; Ziegler, T. *Theor. Chem. Acc.* **1999**, *101*, 396.
(16) (a) Rosa, A.; Ricciardi, G.; Baerends, E. J.; van Gisbergen, S. J. A. *J. Phys. Chem. A* **2001**, *105*, 3311. (b) Baerends, E. J.; Ricciardi, G.; Rosa, A.; van Gisbergen, S. J. A. *Coord. Chem. Rev.* **2002**, *230*, 5.
(17) Velasquez, S. V.; Fox, G. A.; Broderick, W. E.; Anderesen, K. A.; Anderson, O. P.; Barret, A. G. M.; Hoffman, B. M. *J. Am. Chem. Soc.* **1992**, *114*, 7416.
(18) Fischer, M. S.; Templeton, D. H.; Zalkin, A.; Calvin, M. *J. Am. Chem. Soc.* **1971**, *93*, 2622.
(19) (a) Stuzhin, P. A.; Bauer, E. M.; Ercolani, C. *Inorg. Chem.* **1998**, *37*, 1533. (b) Bauer, E. M.; Ercolani, C.; Galli, P.; Popkova, I. A.; Stuzhin, P. A. *J. Porphyrins Phathalocyanines* **1999**, *3*, 371.
(20) Matzumoto, S.; Endo, A.; Mizuguchi, J. *Z. Krystallogr* **2000**, *215*, 182.
(21) Baum, S. M.; Trabanco, A. A.; Montalban, A. G.; Micallef, A. S.; Zhong, C.; Meunier, H. G.; Suhling, K.; Phillips, D.; White, A. J. P.; Williams, D. J.; Barrett, A. G. M.; Hoffman, B. M. *J. Org. Chem.* **2003**, *68*, 1665.
(22) Goslinski, T.; Tykarska, E.; Szczolko, W.; Osmalek, T.; Smigielska, A.; Walorczyk, S.; Zong, H.; Gdaniec, M.; Hoffman, B. M.; Mielcarek, J.; Sobiak, S. *J. Porphyrins Phthalocyanines* **2009**, *13*, 223.
(23) Donzello, M. P.; Ou, Z.; Monacelli, F.; Ricciardi, G.; Rizzoli, C.; Ercolani, C.; Kadish, K. M. *Inorg. Chem.* **2004**, *43*, 8626.
(24) (a) Stillman, M. J. In *Phtalocyanines: Properties and Applications*; Leznoff, C. C., Lever, A. B. P., Eds.; VCH Publisher: New York, 1989; Vol. *1*, pp 133−289. (b) Mack, J.; Stillman, M. J. In *The Porphyrin Handbook*; Kadish, K. M., Smith, K. M., Guilard, R., Eds.; Academic Press: New York, 2003; Vol. *16*, pp 43−116.
(25) (a) Ough, E. A.; Creber, K. A. M.; Stillman, M. J. *Inorg. Chim. Acta* **1996**, *246*, 361. (b) Kobayashi, N. In *Phthalocyanines: Properties and Applications*; Leznoff, C. C., Lever, A. B. P., Eds.; VCH Publisher: New York, 1993; Vol. 2, Chapter 3. (c) Sibert, J. W.; Baumann, T. F.; Williams, D. J.; White, A. J. P.; Barrett, A. G. M.; Hoffman, B. M. *J. Am. Chem. Soc.* **1996**, *118*, 10487. (d) Lee, S.; White, A. J. P.; Williams, D. J.; Barrett, A. G. M.; Hoffman, B. M. *J. Org. Chem.* **2001**, *66*, 461. (e) Kobayashi, N.; Ogata, H.; Nonaka, N.; Luk'yanets, E. A. *Chem.—Eur. J.* **2003**, *9*, 5123. (f) Soldatova, A. V.; Kim, J.; Rizzoli, C.; Kenney, M. E.; Rodgers, M. A. J.; Rosa, A.; Ricciardi, G. *Inorg. Chem.* **2011**, *50*, 1135.
(26) *Electronic Spectra of Phthalocyanines and Related Compounds. Catalogue*; Luk'yanets, E. A., Ed.; NIITEKhIM: Cherkassy, 1989; 94 pages (in Russian).
(27) Kobayashi, N.; Konami, H. In *Phthalocyanines − Properties and Applications*; Leznoff, C. C., Lever, A. B. P., Eds.; VCH Publisher: New York, 1989; Vol. *4*, pp 343−404.
(28) R. P. Linstead, R. P.; Halley, M. *J. Chem. Soc.* **1952**, 4839.
(29) Lever, A. B. P *Adv. Inorg. Chem. Radiochem.* **1965**, *7*, 27−114.
(30) Mikhalenko, S. A.; Luk'yanets, E. A. *Zh. Obshch. Khim.* **1969**, *39*, 2554.
(31) Galpern, M. G.; Luk'yanets, E. A. *Zh. Obshch. Khim.* **1969**, *39*, 2536.
(32) (a) Rosa, A.; Ricciardi, G.; Baerends, E. J.; van Gisbergen, S. J. A. *J. Phys. Chem. A* **2001**, *105*, 3311. (b) Baerends, E. J.; Ricciardi, G.; Rosa, A.; van Gisbergen, S. J. A. *Coord. Chem. Rev.* **2002**, *230*, 5.
(33) Rosa, A.; Ricciardi, G.; Gritsenko, O.; Baerends, E. J. *Struct. Bonding (Berlin)* **2004**, *112*, 49.
(34) Lee, A.; Kim, D.; Choi, S.-H.; Park, J.-W.; Jaung, J.-Y.; Jung, D. H. *Mol. Simul.* **2010**, *36*, 192.
(35) Perdew, J. P.; Burke, K.; Ernzerhof, M. *Phys. Rev. Lett.* **1996**, *77*, 3865.
(36) Delley, B. *J. Chem. Phys.* **1990**, *92*, 508.